Hindawi Publishing Corporation
Advances in Power Electronics
Volume 2010, Article ID 546529, 13 pages
doi:10.1155/2010/546529

Research Article

A Loosely Coupled Planar Wireless Power Transfer System Supporting Multiple Receivers

Zhen Ning Low, Joaquin Jesus Casanova, and Jenshan Lin

Department of Electrical and Computer Engineering, University of Florida, Gainesville, FL 32611-6550, USA

Correspondence should be addressed to Zhen Ning Low, zhenning@ieee.org

Received 9 July 2009; Revised 19 February 2010; Accepted 16 March 2010

Academic Editor: Chang Ming Liaw

A high-efficiency wireless power transfer system which is capable of supporting more than one receiver using class E operation for transmitter via inductive coupling has been designed and fabricated. The design approach of the system is also presented in this paper. The system requires no complex external control system but relies on its natural impedance response to achieve the desired power delivery profile across a wide range of load resistances while maintaining high efficiency to prevent any heating issues. A switch circuit is used to decouple the fully charged receiver from the system so that power delivery to the other receiver can be improved. The fabricated system at 12 V supply voltage is compact and capable of approximately 2.5 W of power delivery to each of the two receivers in a dual receiver setup and 5 W to a single receiver alone or when the other receiver is decoupled by the receiver switch. During high-power delivery state, the system efficiency is between 67.5% and 77.5%.

1. Introduction

Recently, the emergence of various wireless power technologies [1] to eliminate the "last cable" has generated significant research interest in this area. Inductive coupling has been one of the leading candidates in achieving wireless power transfer at power levels ranging from several microwatts to thousands of watts [2–15]. Using near-field operation at frequencies below 1 MHz significantly lowers the probability of interference and RF safety issues since the wavelength is extremely long and radiation is limited. However, unlike far-fields techniques, near-field techniques are extremely sensitive to the loading condition, that is, the number of receivers and the impedance of each one. To date, there have been limited studies on analyzing the power delivery of a planar inductive coupling system to multiple independent receiving units (e.g., multiple cell phones) via a single transmitting unit for consumer electronics applications. Research work on multiple receivers driving a single common load has been reported in [13–15] where the multiple receiving units can be turned on and off to control the power handling of the system. Although [16] shows the potential of supporting multiple receivers on a single transmitting platform, the analysis of the power delivery to a varying load was not presented.

In this paper, additional background theory of [2] will be covered in Section 2. The design approach of the wireless power system, which is different from the method proposed in [2], is covered in Section 3. A switch which can be used as a series switch or shunt switch and capable of handling both high voltage and current using a low voltage control signal is presented in Section 4. The switch is used to decouple the receiving unit that is connected to a fully charged device using the decoupling architecture proposed in [13–15] in a shunt configuration. The analysis of the switch performance as part of the decoupling architecture is presented in Section 5. Experimental verification in Section 6 shows that the system is able to achieve a desirable power delivery response across a wide range of load resistances without any control mechanism or feedback loop. In addition, measurement results on how multiple loads will affect the power delivery and efficiency are also presented in Section 6.

2. Background Theory

2.1. Inductive Coupling. Wireless power transfer of the system described in this paper is achieved via magnetic induction between two air core coils. Appropriate shielding [17] at the expense of weight and thickness can be used to

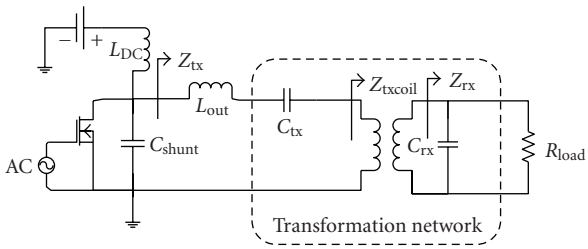

Figure 1: Simplified schematic of wireless power transfer system using series-parallel transformation network and class E transmitter. Z_{tx}: impedance looking into the transmitter load network. Z_{txcoil}: impedance looking into the transmitting coil. Z_{rx}: impedance looking into receiver network. R_{Load} is the equivalent resistance looking into the rectifier.

make the system more robust in environments where the system's magnetic field is likely to interact with other nearby objects. However, shielding is beyond the scope of this paper and it is assumed that the system is adequately shielded from structures and materials that may significantly affect the system performance. This can be achieved by using magnetic materials such as ferrites.

Since the receivers are intended to be integrated into portable devices, it is unlikely that the coil of the receivers will be overlapping each other. Therefore, the mutual inductance between the receiving coils can be neglected as the electromagnetic coupling between the receiving coils, when separated by at least 10% of the largest dimension of the receiving coils, will be significantly weaker than the coupling between the transmitting and receiving coils. The voltage and current characteristics of the transmitting coil and a number (X) of receiving coils can be described using the following equations [3, 8]:

$$V_1 = j\omega M_{11} I_1 + j\omega \sum_{N=1}^{X} M_{1N} I_N, \tag{1}$$

$$V_N = j\omega M_{N1} I_1 + j\omega M_{NN} I_N, \tag{2}$$

$$M_{1N} = k_N \sqrt{M_{11} M_{NN}}, \tag{3}$$

where V_1 is the voltage at the transmitting coil (Figure 2), I_1 is the current at the transmitting coil (Figure 2), V_N is the voltage at the Nth receiving coil (Figure 2), I_N is the current at the Nth receiving coil (Figure 2), M_{11} is the self inductance of the transmitting coil, M_{NN} is the self inductance of the Nth receiving coil, $M_{1N} = M_{N1}$ is the mutual inductance of the transmitting coil and the Nth receiving coil, k_N is the coupling coefficient between the transmitting coil and the Nth receiving coil.

By Ohm's law:

$$Z_{tx} = R_{tx} + jX_{tx} = \frac{V_1}{I_1}, \tag{4}$$

$$Z_{rxN} = R_{rxN} + jX_{rxN} = \frac{V_N}{I_N}. \tag{5}$$

Using (1), (2), (4) and assuming a time-harmonic operation with frequency ω, Z_{tx} can be derived as

$$Z_{tx} = \sum_{N=1}^{X} \frac{\omega^2 M_{1N}^2 R_{rxN}}{R_{rxN}^2 + (\omega M_{NN} + X_{rxN})^2} + j\left(\omega M_{11} - \sum_{N=1}^{X} \frac{\omega^2 M_{1N}^2 (\omega M_{NN} + X_{rxN})}{R_{rxN}^2 + (\omega M_{NN} + X_{rxN})^2}\right). \tag{6}$$

The above analysis of the coupling neglects any 2nd order effects such as skin depth and proximity effects. Litz wires can be used to mitigate such effects.

2.2. Impedance Transformation Network. The purpose of impedance transformation network on the primary and secondary sides of the coupling is to achieve maximum power transfer and efficiency by operating within the optimum impedance range looking into the transmitter load network [18–20] over a wide range of load resistance at receiver.

Four possible topologies of the single-element transformation network have been discussed in [2] and the series-parallel and series-series topology have also been analyzed in greater depth in [21]. It has been discussed in [2] that a parallel receiver transformation network is preferred over a series receiver transformation network due to low coupling coefficient. For the transmitter transformation network, a series or parallel topology can be used. Instead of selecting a parallel topology in [2], a series topology is selected to reduce component count. The design rules of the planar wireless power system will be different from those presented in [2] and will be discussed in Section 3. The C_{tx} as shown in Figure 1 is part of the impedance transformation network and also serves as part of the output filter of the class E amplifier (in series with L_{out}). To maintain an ideal efficiency above 95%, the allowable variation of load resistance of an ideal class E amplifier should be kept within +55% and −37% [19].

2.3. Challenge of Power Transfer to Multiple Receivers. The block diagram of the wireless power system transferring power to multiple receivers using inductive coupling is shown in Figure 2. A class E amplifier with an input clock as shown in Figure 1 is used as the inverter.

Delivering power to a device which has a high-efficiency switching regulator at the input is challenging. This is because a typical buck switching regulator, requiring a higher input voltage to operate, tends to "amplify" the load resistance. The "amplification" of load resistance will tend to "choke" the other receivers when the wireless power system is transferring power to multiple receivers, especially when one of the receivers is in a high-resistance/trickle charge state. In order to achieve considerable power delivery to other receivers, the fully-charged receiving device needs to decouple itself from the system. The decoupling can be achieved by using a switch, as proposed in [13–15].

The regulator input resistance can be several ohms at a high-power charging state or thousands of ohms during trickle charge state. In addition, developing a robust control system to avoid the bifurcation phenomena [8–10] can increase the complexity of the system significantly. The

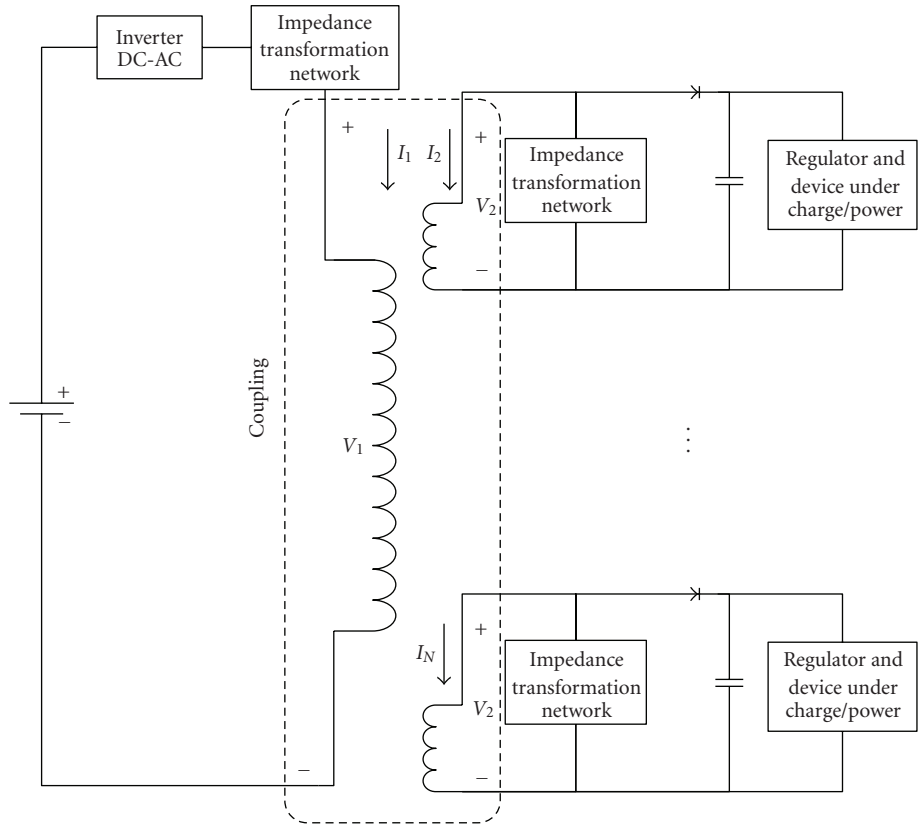

Figure 2: Block diagram of the wireless power transfer system delivering power to multiple receivers using inductive coupling.

complexity will increase exponentially with the number of receivers. Therefore, it is desirable for the wireless power system to have a natural response without any external control or feedback such that its power delivery property closely matches a typical wall mounted DC supply and is transparent to the device.

A robust wireless power transfer system must be able to provide a significant amount of translational freedom such that the power transfer is insensitive to the placement of the device. In addition, it will be desirable for the system to concurrently power or charge multiple devices. The convenience for users of portable wireless devices is the key feature of the proposed wireless power transfer system. Therefore, the receiving coil should be significantly smaller than the transmitting coil, resulting in a generally weak/loose coupling with a coupling coefficient of less than 0.25, which was determined experimentally for receivers with size smaller than 20% of the transmitting coil size. Under this condition, the interaction between the coils cannot be treated like an ideal transformer. It is due to the weak coupling, as discussed in [2], that a parallel capacitor across the receiving coil is more suitable. Similar implementations using a parallel capacitor can be found in [9, 10] and [13–15].

3. Design Approach

The design of the proposed wireless power system is started by setting constraints of the dimensions of the transmitting and receiving coils as well as the operating frequency. Although higher operating frequency will reduce component value and size, switching and parasitic losses will also increase. An operating frequency of 240 kHz is used for the system in this paper. To simplify the analysis, the load resistance is defined as the equivalent resistance looking into the rectifier instead of after the rectifier. To minimize space usage as well as ease of integration into the target device, the receiving coil is typically tightly wound. However, the windings of the transmitting coil are very different from the receiving coil. The gaps between each turn of the transmitting coil are spaced in a manner to achieve uniform field distribution and consistent performance regardless of the placement of the receiving coil. A 13-turn 20 cm × 20 cm transmitting coil is used for the experimental verification in Section 6. The layout and field distribution of the transmitting coil can be found in [22].

Key parameters of the coils including self inductances, mutual inductance, and parasitic resistances can be extracted by measuring the fabricated coil with an impedance analyzer or analyzing with electromagnetic simulation tools. The coils to be used for the experimental verification in Section 6 were fabricated using 100/40 round served Litz wires to mitigate proximity effect and skin effect. The 100/40 round served Litz wires consists of 100 strands of 40 gauge wires insulated from each other. The self inductance of the transmitting coil is 45.3 μH with a parasitic resistance of 0.5 Ω. The self inductance of the receiving coil is 5.8 μH with a parasitic

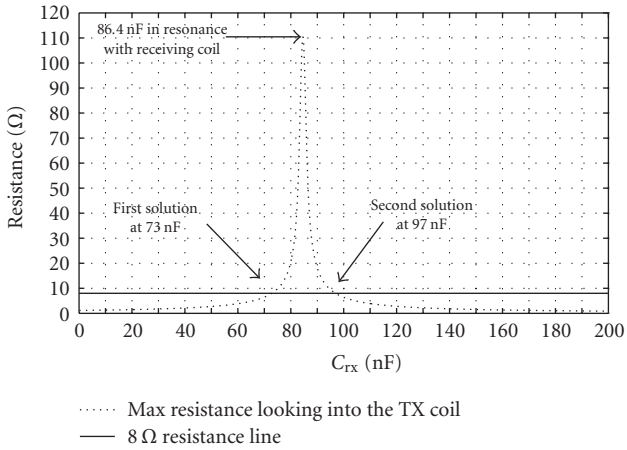

Figure 3: Resistance response looking into the transmitting coil with respect to C_{rx}.

resistance of 0.1 Ω. Mutual inductance between the coils is 2.8 μH with a coupling coefficient of 0.1727. Both of the coils were measured using the HP4192A LF Impedance Analyzer.

3.1. Determination of C_{rx} Value. The capacitance value is selected based on the inductance of the receiving coil as well as the mutual inductance between the coils. Although it would be desirable to achieve a maximum resistance looking into the transmitting coil across a wide range of load resistances [2], the resistance variation looking into the transmitting coil might become too big. A shunt capacitor is connected across the transmitting coil to "compress" the resistance, resulting in a parallel-parallel impedance transformation network topology. Therefore, it is necessary to select a capacitor value that will generate the desirable resistance range [19] looking into the transmitter load network and shift the reactance value to achieve a desirable phase response and a desirable power delivery profile, which can be accomplished by varying C_{tx} or L_{out}. In order to determine the range of resistance looking into the transmitting coil, an appropriate L_{out} value needs to be selected first. The class E transmitter requires a minimum loaded Q of 1.7879 to operate [18]. For this design, a 10 μH inductor (RL-5480-5-10 from Renco) is selected. The inductor has low parasitic resistance of 0.16 Ω at 240 kHz and is considerably small in size (15.875 mm diameter and 17.78 mm height). The effective inductance of the inductor is 9.5 μH at 240 kHz due to parasitic capacitance.

Based on the minimum loaded Q from [18], the resistance looking into the transmitting coil should not be larger than 8 Ω. However, it will be desirable to achieve a maximum resistance as high as possible to reduce losses through the parasitic resistances. Therefore, by performing a sweep on the receiver capacitor from 0.1 nF to 200 nF, Figure 3 illustrates that there are two possible solutions, 73 nF and 97 nF to achieve a resistance of 8 Ω. It can also be seen from Figure 3 that the peak resistance occurs at the 86.4 nF, which indicates that the capacitor is in resonance with the receiving coil. Although this operating point can give maximum resistance looking into transmitting coil, the class E amplifier would have limited operating load resistance range [19]. Therefore, a bounded resistance range is required in this system.

Although both capacitance values of C_{rx}, 73 nF and 97 nF, provide the same resistance response looking into the transmitting coil, the reactance trend is different. Using the capacitance value of 73 nF results in an increasing trend of reactance response converging to approximate 82 Ω as shown in Figure 4. On the other hand, a larger capacitance value of 97 nF will result in a decreasing trend of reactance response converging at approximately 51 Ω as shown in Figure 4. According to (7), increasing the reactance while keeping the resistance relatively unchanged will decrease the power delivery. Therefore, in order to obtain the desirable trend of decreasing power delivery with respect to the increase of load resistance the first solution of 73 nF is selected

$$P = \frac{V^2}{Z_{tx}} \cos\theta = \frac{V^2 R_{tx}}{{Z_{tx}}^2}. \tag{7}$$

Based on the selected receiver capacitance value, the coupling efficiency with respect to load resistance as shown in Figure 5 can be calculated using the parasitic resistance of the coils shown in Table 1 as ohmic losses. Radiation losses are assumed to be minimal as the radiation resistance is negligible at 240 kHz. Coupling efficiency peaks at close to 90% at a load resistance of 30 Ω. Although efficiency rolls off to around 36% at 1 kΩ, power delivered to the load resistance is very low and does not present heating problems to the system. The decrease in power delivery as shown in Figure 5 when load resistance increases is desirable as it helps to regulate the power during trickle charge.

3.2. Determination of C_{tx} Value. Figure 6 shows the phase response of Z_{tx} with respect to load resistance for different C_{tx} values. High efficiency is achieved at a range of phase angles from 40° to 70° [22]. Therefore, any value above 7 nF can be used for C_{tx}. Since the coil inductance is large, the phase response will be sensitive to the component values and a large phase response swing can be observed when C_{tx} is changed from 6 nF to 7 nF. C_{tx} is selected to be 8 nF to achieve both maximum power delivery and stability. It should be noted that a higher C_{tx} can be selected to limit the power delivery as shown in (7), which was also discussed in [10, 19]. In addition, the load resistance should be kept approximately above 25 Ω where the power peaks at the lowest phase angle. Any decrease in load resistance below the peaking point will overload the system and reduce power output and efficiency.

3.3. Determination of C_{shunt} Value. Once the values of the inductors and capacitors in the transmitter load network and the receiver network are determined, the remaining step is to determine C_{shunt} to achieve ZVS and ZDS operations so as to minimize switching losses. The optimum C_{shunt} value can be determined using the equations derived in [19, 20] which are implemented in a Matlab code. The optimum C_{shunt} is found to be 10 nF and the variation of transistor drain voltage versus load resistance is shown in Figure 7. It can be seen that the transistor drain voltages are kept very

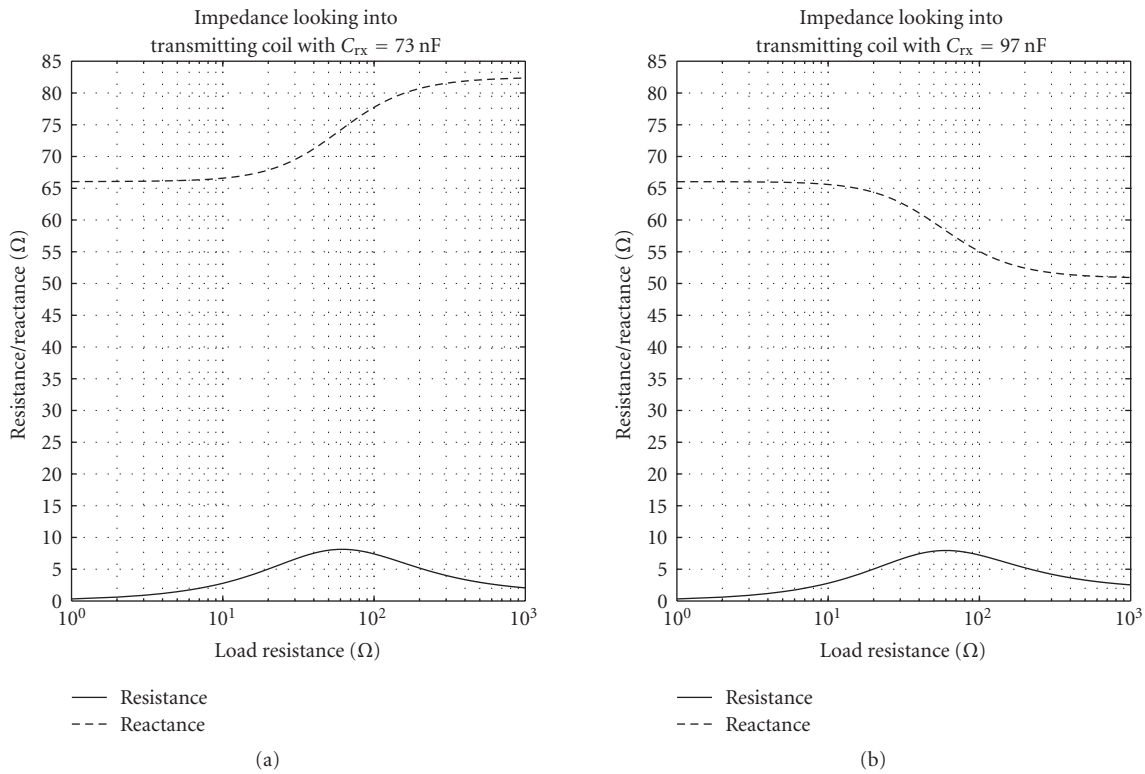

Figure 4: Resistance and reactance responses looking into the transmitting coil with receiver capacitance of 73 nF and 97 nF.

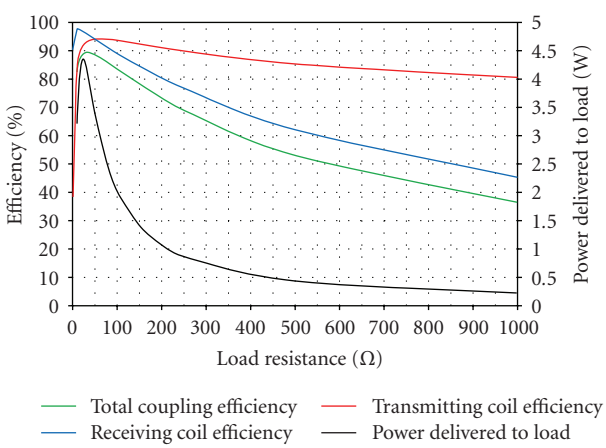

Figure 5: Coupling efficiency with respect to load resistance.

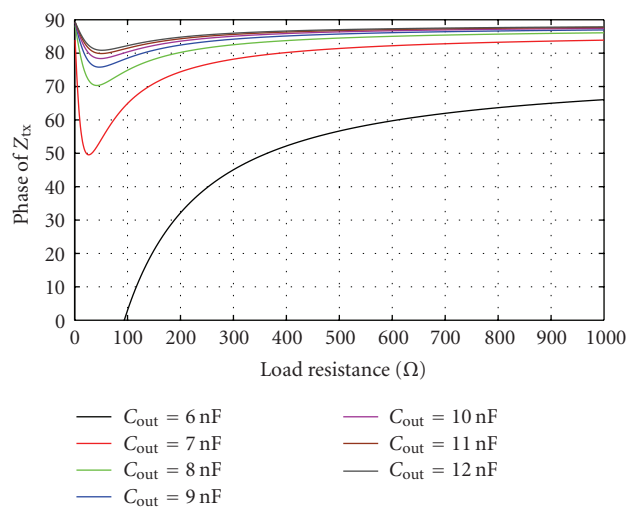

Figure 6: Z_{tx} phase response with respect to load resistance for various C_{tx} capacitance values.

close to zero when the transistor is being switched on at a phase of 180°. In addition, the negative voltages are restricted by the built-in diode's turn-on voltage at around −1.3 V.

4. Receiver Switch Circuit Design

Since the receiver is designed for use in a portable device such as a cellular phone or an mp3 player powered by a 3 V battery, the switch needs to be compact and controllable by a low voltage supply of 3 V or less. Although most electromechanical switches are able to tolerate large voltages and currents, they are typically large and generate a "clicking" sound during switching which is not desirable. Off-the-shelf solid state switches are typically designed for 50/60 Hz AC line application without good high frequency response and are relatively large in size. It is possible to find switches which operate at high frequencies but the power handling starts to drop with increasing frequency [23] unless expensive novel materials are used as shown in [24]. Most importantly, it is difficult to control the switch

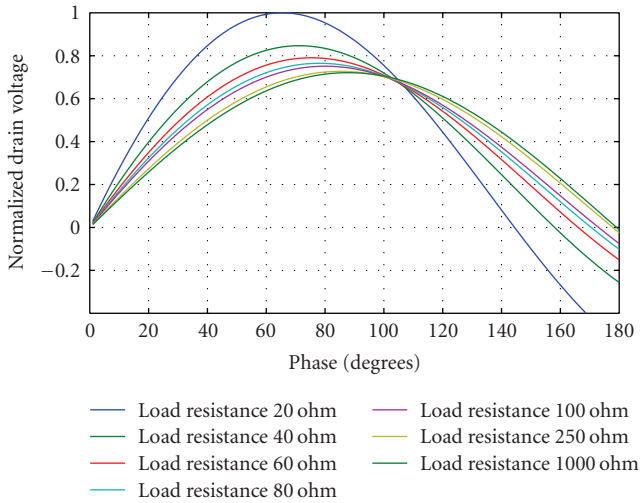

Figure 7: Transistor drain voltage waveform for different load resistance. (C_{shunt} = 10 nF).

with voltages lower than the voltage being switched using a simple transmission gate topology or switch transistors. The discussion of the switch circuit in this section is independent of the decoupling architecture and can be used in either series or shunt topology.

The block diagram of the switch circuit is shown in Figure 8. It consists of a transmission gate with an NMOS and a PMOS in parallel. A Schottky diode must be added either before or after the transistor to counter the effect of the body diode of the power MOSFET. The Schottky diode selected must have power handling capability comparable to the body diode of the transistor. The control signals to the gate of both of the transistors are provided via their respective switch control network. Two rectification circuits extract the maximum voltage and minimum voltage of the input AC voltage. The maximum and minimum voltages are used as inputs for their respective switch control networks in a cross-coupled topology. Based on the control signal provided by the receiver, the switch control network will switch between the maximum voltage and the minimum voltage to either turn the transmission gate on or off.

Schematic of the switch circuit is shown in Figure 9. A single package dual N and P channel MOSFET (IRF7343) from International Rectifier is used. The Schottky diode MBRA340T3, is selected for both the rectification network diode and switch. Notation for resistors and capacitors are in the form of RX_X and CX_X. The number after the underscore is used to differentiate between the two similar switch control networks, namely channel 1 for the P channel MOSFET of the transmission gate and channel 2 for the N channel MOSFET of the transmission gate. Values for $C1$, $C2$, $R1$, and $R2$ are 100 nF, 10 nF, 10 kΩ, and 47 kΩ, respectively. The switch circuit does not use any inductors and can be easily integrated monolithically into a chip or a single package solution with the voltage regulator.

Simulation and verification of the switch was carried out using Agilent ADS. The purpose of the analysis is to study the performance of the circuit as a generic switch and not as a specific decoupling mechanism. Transistor and diode models were obtained from the manufacturers to achieve accurate prediction of the performance of the fabricated circuit.

A switch control input waveform that has 0 V for off state and 3 V for on state at a 50% duty cycle and a frequency of 100 Hz is used in the simulation. Figure 10 shows the generated switch control voltage for each respective channel. The switch closing response time for channel 1 is 630 μS and channel 2 is 700 μS. The switch opening response time for channel 1 is 60 μS and channel 2 is approximately 70 μS. The faster switch closing time can be explained by looking at the voltages across $C1$ and $C2$. The voltages are the same when the switch is open and when the switch is closed, $C2$ is charged/discharged via the low resistance path through the transistor. On the other hand, when the switch is opening, $C2$ is charged/discharged via resistor $R1$ which increases the time constant significantly. Finally, Figure 11 shows the output AC waveform of the switch.

5. Receiver Architecture with Decoupling Capability

Figure 12 shows the receiver architecture with decoupling capability, which has been discussed in [13–15]. An additional inductor can be added at the output of the diode before Cdc to improve the efficiency and reduce the ripple level. By shorting the receiving coil, the receiver coil sees a short. Therefore, R_{rx} and X_{rx} in (6) will be extremely small such that we can assume them to be zero. Let X_{rx} in (6) be zero

$$Z_{\text{tx}} = \frac{\omega^2 M_{12}^2 R_{\text{rx}}}{R_{\text{rx}}^2 + (\omega M_{22})^2} + j\left(\omega M_{11} - \frac{\omega^3 M_{12}^2 M_{22}}{R_{\text{rx}}^2 + (\omega M_{22})^2}\right). \tag{8}$$

Next let R_{rx} in (8) be zero

$$Z_{\text{tx}} = j\left(\omega M_{11} - \frac{\omega M_{12}^2}{M_{22}}\right). \tag{9}$$

Substituting (3) into (9)

$$Z_{\text{tx}} = j(\omega M_{11} - \omega k^2 M_{11}). \tag{10}$$

In order for the system to be able to support multiple devices and provide sufficient lateral freedom, it is reasonable for the coupling coefficient to be much less than 0.25. By assuming a coupling coefficient of 0.25, k^2 will be 0.0625 which is much smaller than 1. Therefore, if the receiving coils are short-circuited under loose coupling condition, the transmitter is approximated seeing only the self inductance of the transmitting coil as if the system is not loaded.

Second, the switch's natural state is open. Therefore, the receiver will allow power to pass through when the control port is left floating. This is critical especially when the battery on the receiver is fully drained and is unable to control the switch.

Figure 13 shows the test bench to verify the performance of the switch when used in this specific scenario. A similar

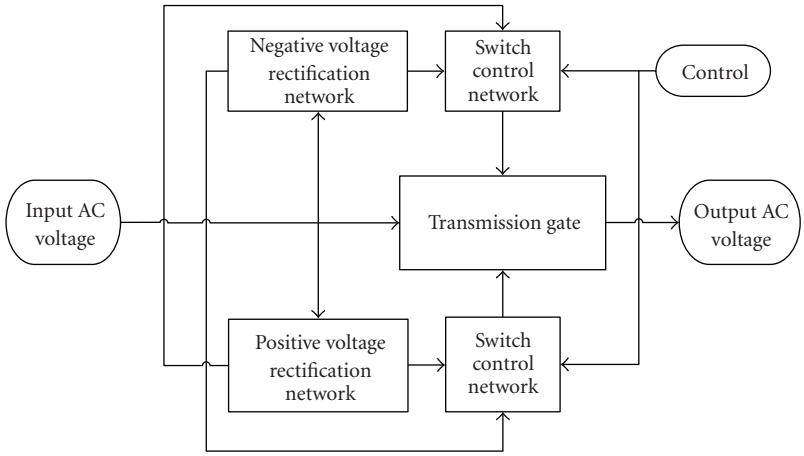

Figure 8: Block diagram of the switch circuit.

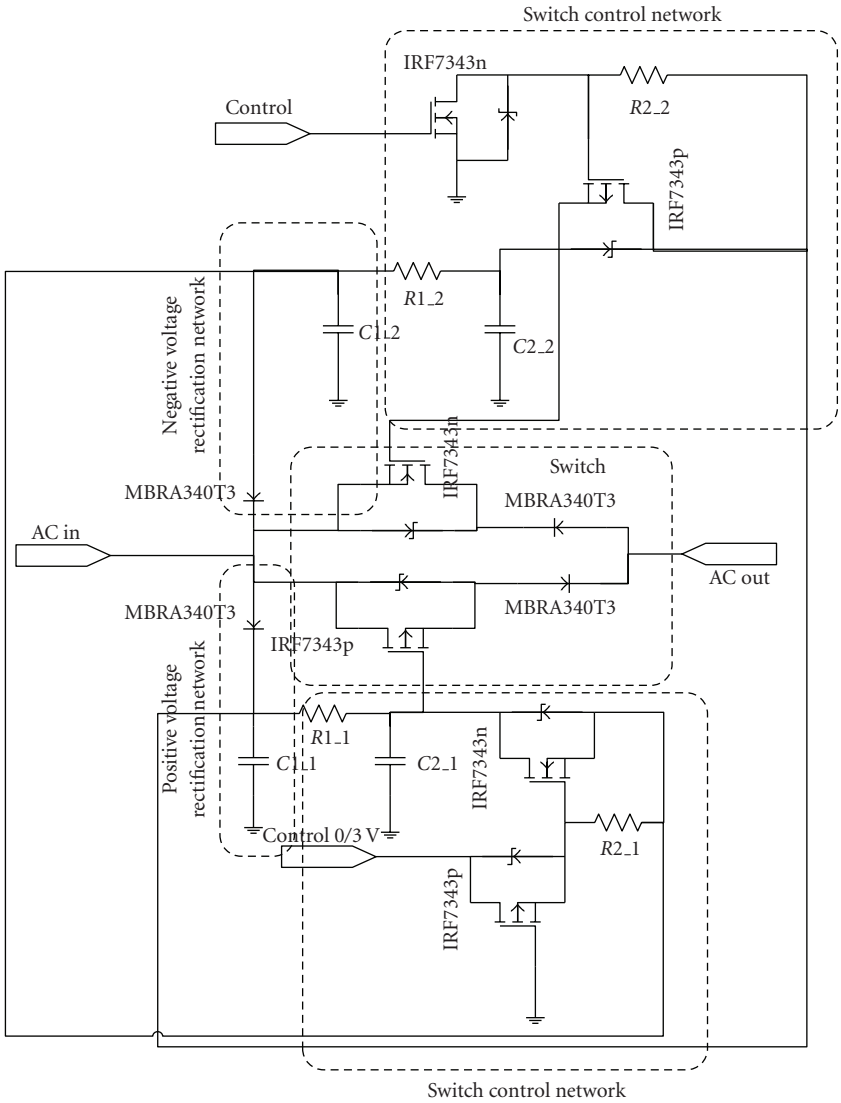

Figure 9: Schematic of the switch circuit.

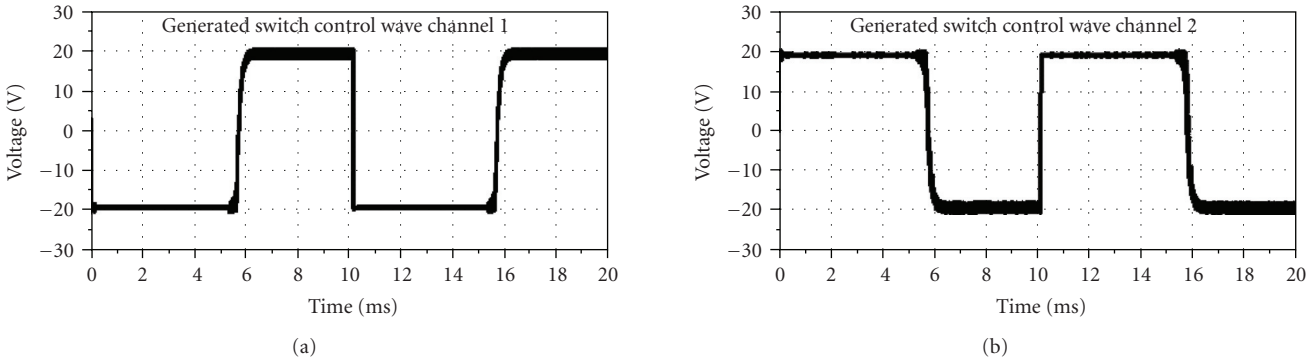

Figure 10: Generated switch control waveform for channel 1 (P channel MOSFET of the transmission gate) and switch control waveform for channel 2 (N channel MOSFET of the transmission gate).

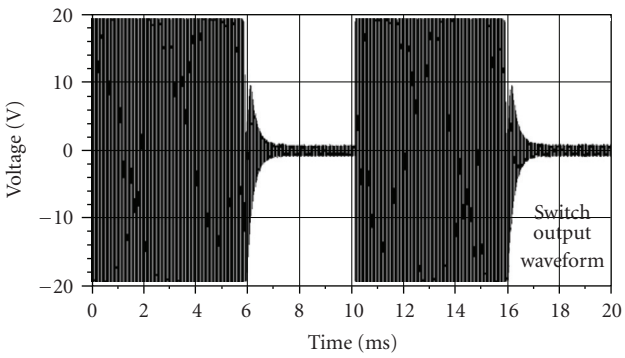

Figure 11: Output waveform of the switch.

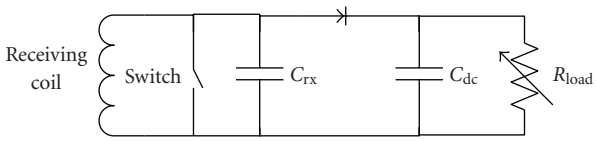

Figure 12: Receiver architecture with decoupling capability.

clock control source is used as well. The switch circuit in Section 4 is converted to the modular block $X1$. Instead of using a full class E driver, the transmitter is simplified as an AC current source with 1 A peak current at 240 kHz. The transmitter coil is modeled as inductor $L1$ and receiving coil as inductor $L2$, mutual inductance is modeled via "Mutual1" block.

Figure 14 shows the simulation results of the test bench of Figure 13. As predicted in Section 4, the switch closing time is faster than the opening time, resulting in a faster decoupling response time. Although the receiver is supposed to be fully decoupled when the switch closes, a 0.5 V DC voltage still can be observed at load. This is because the switch is not an ideal switch and a potential drop will be observed across the parasitic resistance of the transmission gate transistor as well as the series diodes used to counter the effect of the body diode. The 0.5 V DC voltage should not be a concern because it is not sufficient to turn on the voltage regulator which is typically used to provide a stable DC voltage. From the simulation results, it can be concluded that the switch circuit can be used in scenarios where a control voltage is significantly smaller than the input AC voltage at high frequencies regardless of topologies. Efficiency of the switch can be inferred from the experimental results in Section 6.

6. Experimental Verification

The class E transmitter test system operating at 240 kHz was fabricated using the IRLR/U3410 power MOSFET. A 13-turn 20 cm × 20 cm transmitting coil [22] and two 6-turn 9 cm × 6 cm receiving coils were used. The platform is capable of simultaneously charging up to four independent devices. Although it is possible to extend the experiment to more than two receivers, for better understanding of the system response and easier analysis, experiments of charging two receivers were conducted. A Matlab code was also written based on the equations derived in [19, 20] to study the efficiency and power delivery. All measurements and simulation results are based on a 12 V power supply. The 12 V power supply is selected because the supply voltage is readily available from the DC supply plugs in vehicles and several other AC-DC converters.

Table 1 shows the value of each component used in the experiment. Component values are selected by matching the closest available component value and further tuned to achieve optimum performance. C_{rx} is selected to be 75 nF. Since the switch contributes 3.5 nF of capacitance and the rectifier contributes another 3.5 nF of capacitance, a 68 nF capacitor is used to achieve an effective capacitance of 75 nF. Capacitance contributed to the receiver due to the switch and rectifier is measured using the HP4192A LF Impedance Analyzer in small signal operation. Therefore, the actual capacitance under large signal operation will be slightly different depending on the load conditions and voltage at the switch and rectifier. In order to reduce losses through parasitic resistance, low loss polypropylene capacitors are used.

Figure 15 shows the photograph of the test setup with two receivers on the packaged transmitting coil. The vertical separation between the transmitting coil and receiving coils is about 2 mm. The locations of receivers on the transmitting coil were fixed by the blue tapes to ensure the same conditions for all measurements.

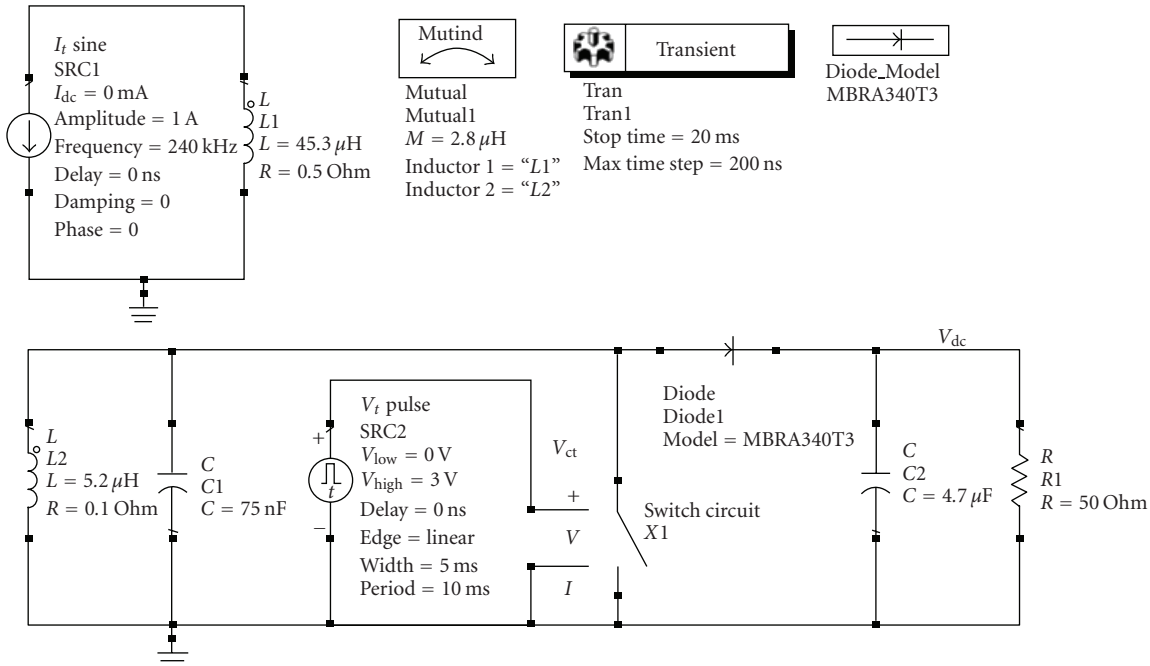

Figure 13: ADS schematic of test bench for receiver architecture in Figure 12.

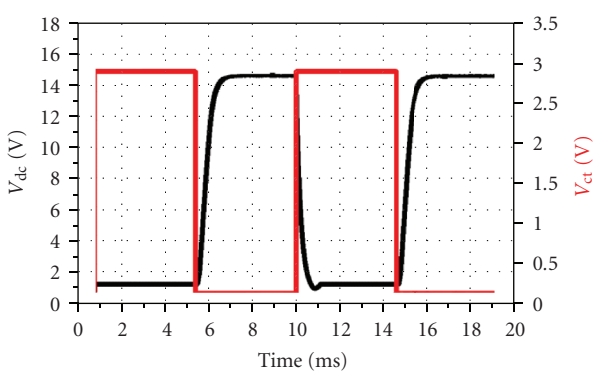

Figure 14: Simulation results of test bench (Figure 16). Red: Low voltage control signal. Black: Receiver rectified voltage.

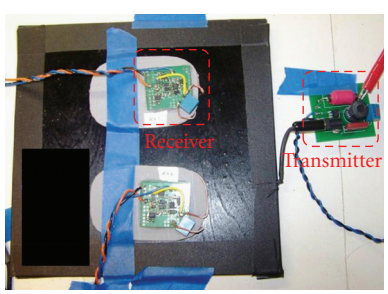

Figure 15: Photograph of a test setup with two receivers on the packaged transmitting coil.

Table 1: Component values.

	Calculated	Experimental	% Variation
C_{rx}	73 nF	75 nF	+2.7%
C_{tx}	8 nF	9.4 nF	+17.5%
L_{out}	9.5 μH	9.5 μH	0%
L_{out} parasitic resistance	—	0.16 Ω	—
C_{shunt}	10 nF	12 nF	+20%
TX coil inductance	—	45.3 μH	—
TX coil dimension	—	20 cm × 20 cm	—
TX coil parasitic resistance	—	0.5 Ω	—
RX coil inductance	—	5.8 μH	—
RX coil dimension	—	9 cm × 6 cm	
RX coil parasitic resistance	—	0.1 Ω	—
Mutual inductance	—	2.8 μH	—
L_{DC}	—	500 μH	—

Power delivery to the receiver and end-to-end DC efficiency versus load resistance of a one-to-one setup is shown in Figure 16. Measurements are conducted by connecting the receiver to a rheostat for which the resistance is varied manually in predetermined steps. The simulation and measured trend of a single receiver setup agree well with peak measured power at around 4.4 W. The end-to-end DC efficiency can be split into three subefficiency blocks. They are transmitter/PA efficiency, coupling efficiency and receiver efficiency (inclusive of receiver transformation network and rectifier). Although the class E power amplifier can achieve an efficiency close to 100%, the power amplifier is driving a very low load (typically <10 Ω). This results in the losses across L_{out} and C_{tx} to be more significant. Taking into account the losses of L_{out} and C_{tx}, the efficiency of the

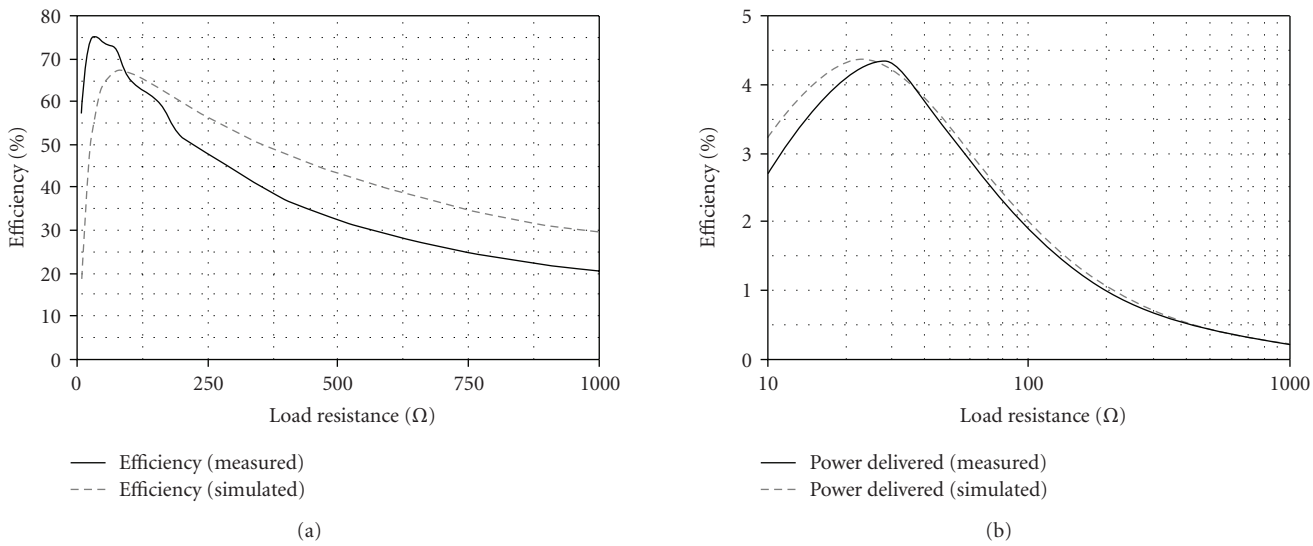

Figure 16: (a) System efficiency versus load resistance for a 1 to 1 setup (simulated and measured) (b) Power delivery versus load resistance for a 1 to 1 setup (simulated and measured).

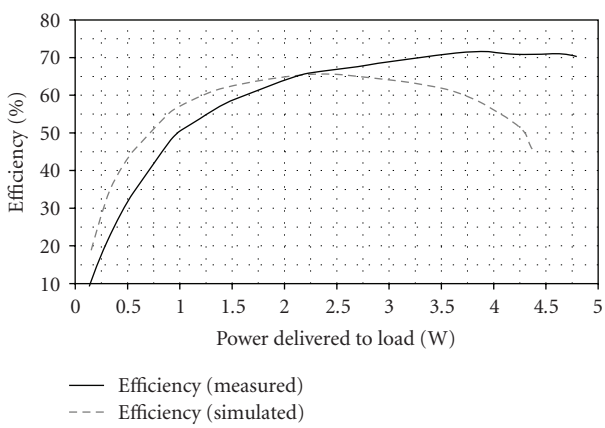

Figure 17: System efficiency versus power delivery for a 1 to 1 setup (simulated and measured).

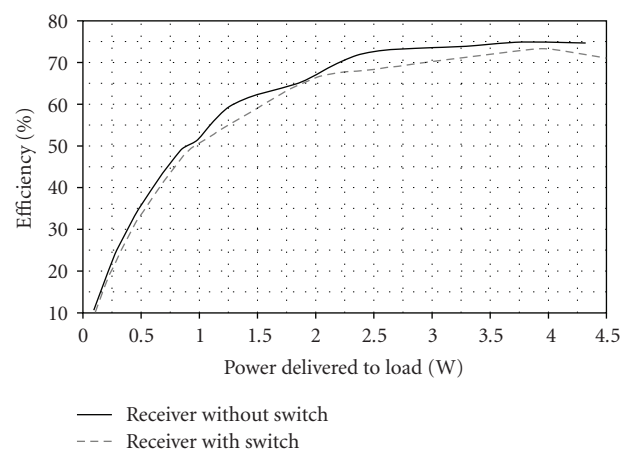

Figure 18: Comparison between receiver with switch and receiver without switch.

transmitter is approximately 90%. The coupling efficiency is already shown in Figure 5. Taking into the account of the losses of C_{rx} and the rectifying diode, the receiver is approximately 95%. This brings the peak end-to-end DC efficiency close to 75%. Figure 17 shows the system efficiency versus power delivery. Simulation and measurement are compared. The discrepancy becomes significant at high power because the transistor and DC feed inductor are assumed to be ideal in the simulation model. The assumption affects the calculated supply current and the calculated efficiency. The simulation model can be further improved by using nonideal models for the transistor and DC feed inductor. Simulation and measurement of power delivery (Figure 16) agree better because power delivery depends on Z_{tx} rather than the transistor during nominal operation.

Figure 18 compares the performance of the receiver with and without the switch. Power delivery capabilities of both receivers are nearly the same, peaking at around 4.5 W with the efficiency of the receiver with switch slightly

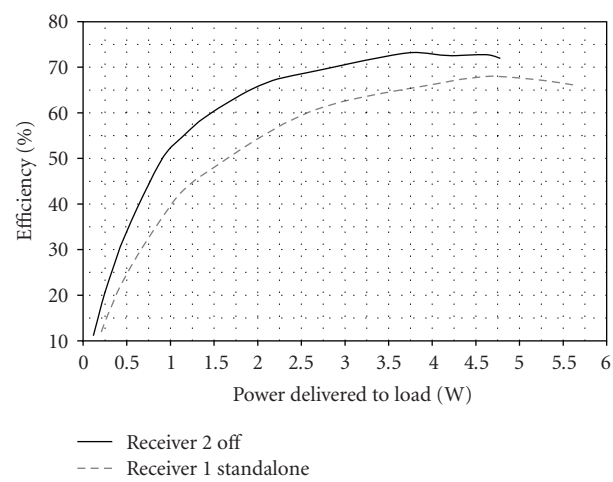

Figure 19: Comparison between single receiver standalone and dual receiver setup with one receiver switched off.

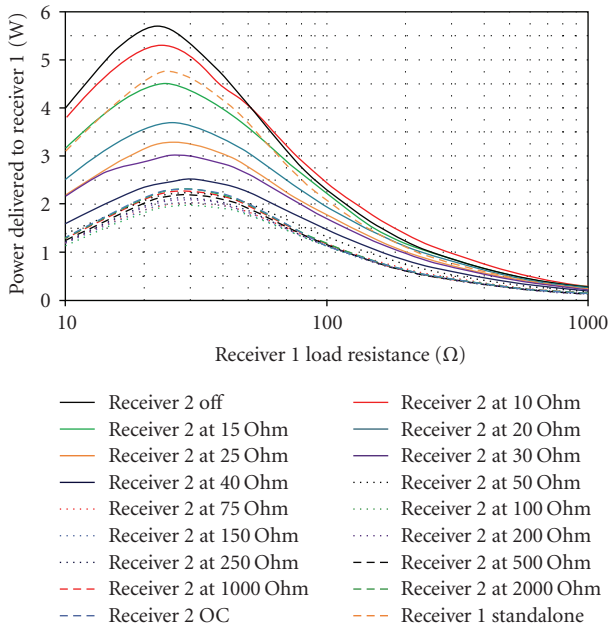

Figure 20: Power delivery to receiver 1 versus its load resistance at different fixed receiver 2 load resistance.

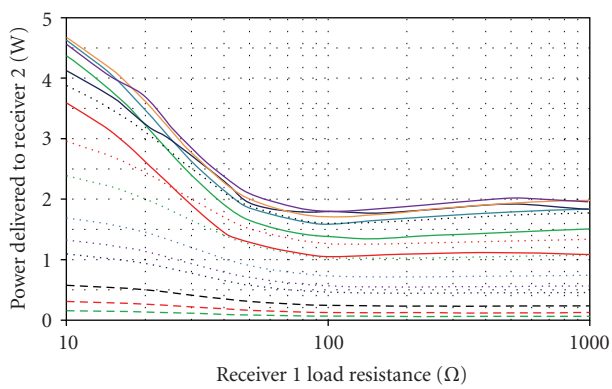

Figure 21: Power delivery to receiver 2 versus receiver 1 load resistance at different fixed receiver 2 load resistance. (same legends as in Figure 20).

lowered by 1% to 2%. The impact of the switch in the receiving mode is minimal because it is in shunt with the receiver. In addition, it can be concluded that the leakage through the switch is negligible. Figure 19 compares the performance of a single receiver with the decoupling switch architecture and dual receiver setup with one of the receivers decoupled from the transmitter. The efficiency degrades by an average of 5% and no more than 10% overall even though the second receiver is turned off. Although the receiver is decoupled from the system, the switch circuitry still has some turn-on resistance when it attempts to short the receiving coil. Therefore, a small amount of power is still dissipated across the switch. This is also observed in the ADS simulation in Section 5 as shown in Figure 14. Although, such performance degradation might be acceptable for a system supporting two devices, the degradation in efficiency would be significant for a system supporting more than three

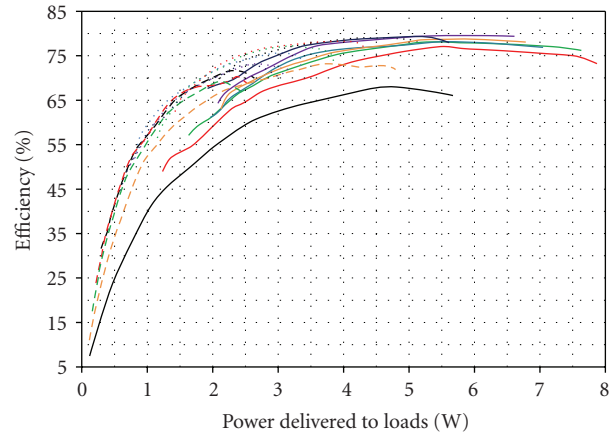

Figure 22: System efficiency versus total power delivery to both receivers with the load resistance of receiver 2 fixed and the load resistance of receiver 1 swept across the stated range for a dual receiver test bench. (same legends as in Figure 15).

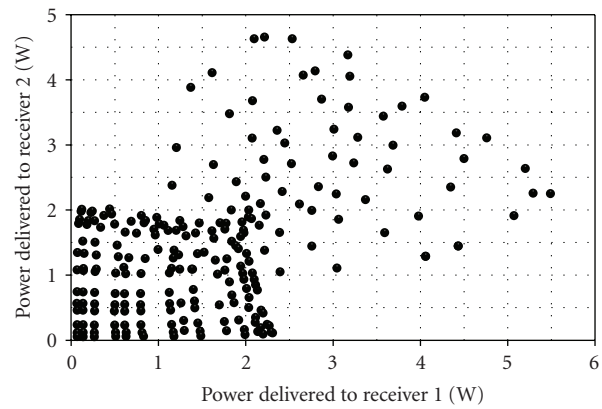

Figure 23: Measured power delivery to a dual receiver system with load resistance varied from 10 Ω to 2000 Ω.

devices. Therefore, selecting a pair of higher performance NMOS and PMOS transistors as well as Schottky diodes will be desirable to maintain an acceptable level of efficiency.

To study the power delivery of a dual receiver platform, the load resistance of one of the receivers (receiver 2) is fixed while the load resistance of the other receiver (receiver 1) is swept across the range of 10 Ω to 2000 Ω in 15 steps (10 Ω, 15 Ω, 20Ω, 25 Ω, 30 Ω, 40 Ω, 50 Ω, 75 Ω, 100 Ω, 150 Ω, 200 Ω, 250 Ω, 500 Ω, 1000 Ω, and 2000 Ω) in experiment using the same method for the single receiver measurement. Figure 20 shows the power delivery to the receiver 1 versus its load resistance at different receiver 2 load resistance values, while Figure 21 shows the power delivery to receiver 2 versus receiver 1 load resistance at different fixed receiver 2 load resistance values. When the load resistance of receiver 2 is kept above 40 Ω, the variation of power delivery to receiver 1 is limited with peak power at around 2.5 W. In addition, power delivery to receiver 2 also stays consistent regardless of the load resistance or power delivery to receiver 1, as long as the load resistance of receiver 1 stays about 40 Ω. To reduce the dependency of the receivers on each other due to

a single driving coil, the minimum load resistance should be greater than 40 Ω. The dependency of the receivers is due to the collective impedance looking into the transmitting coil by the receivers and not the mutual inductance between the receiving coils. The minimum load resistance can be designed by selecting an appropriate receiver regulator and setting the appropriate power delivery profile by changing C_{tx}, as mentioned in [13] and [19], or the supply voltage. This will set the unregulated input voltage before the regulator to achieve the specified load resistance looking into the regulator while it is at its maximum power delivery. The experimental verification and analysis is limited to two receivers but similar trends are expected for multiple receivers of three or more.

Once the fully charged receiver (receiver 2) is decoupled from the system using the switch circuit, power delivery to the other receiver (receiver 1) increases significantly with respect to case of a standalone receiver. The increase in power is due to the intrinsic nature of the transmitting coil and class E PA. The presence of metal from the receiver device (phone/PCB) reduces the self inductance of the transmitting coil, which lowers the phase angle of the load seen by the class E power amplifier, thus increases power delivery. Although the increase in power delivery might be acceptable for a system supporting two devices, it can be too much for a system supporting more than three devices. This effect can be mitigated by providing additional ferrite shielding on the receiving coil so that the presence of the metal from the receiver device will have minimal impact on the self inductance of the transmitting coil. In addition, it can be seen from Figure 20 and Figure 21 that decreasing the load resistance of one receiver increases the power to the other receiver. This can be explained by Figure 4 for which the imaginary component of Z_{txcoil} (shown in Figure 1) reduces across the range of load resistances of 20 Ω to 200 Ω. The final reduction of the imaginary component of Z_{txcoil} by a short-circuited load resistance can be obtained from (10). Therefore, the switch circuit can be used to prevent the receiver that is fully charged to "choke" the other receiver of the power it needed. This will mitigate the effect of reduced charge rate for the receiving devices so that the system will be able to deliver sufficient power to the receiver.

Figure 22 shows the system efficiency versus total power delivered to the loads with receiver 2 fixed at a specific load resistance while sweeping the resistance of receiver 1 from 10 Ω to 2000 Ω. System efficiency is above 55% for power delivery above 2 W. Although the efficiency starts to degrade significantly at lower power delivery, the absolute system power loss is low. Therefore, no heating issues were observed during the experiment. All components were operating below 36°C.

Figure 23 shows the measured power delivery space of receiver 1 and receiver 2. Under all loading conditions the guaranteed power delivery is approximately 2 W. The guaranteed power delivery can also be observed in Figure 20 in another form. Therefore, the system is capable of delivering 2 W of power under all conditions which is close to the specified power delivery of 2.5 W in the design. Higher power delivery can be achieved by reducing the capacitance of C_{tx} slightly [10] and [19] or by increasing the supply voltage. Care must be taken during reduction of C_{tx} to keep the phase of Z_{tx} within the high-efficiency/low loss operation above 40° [19].

7. Conclusion

A design approach using the series-parallel impedance transformation network topology is presented. A switch is also presented to achieve the decoupling mechanism based on the technique found in [13–15]. By decoupling a fully charged receiver from the system, power delivery to the other receiver can be improved. Experimental results verified the design. The fabricated system operating at a 12 V supply is capable of delivering nearly 2.5 W power to each receiver for a dual receiver setup under any loading conditions and 5 W to a single receiver alone or when one of the receivers is decoupled by the switch. System efficiency is higher than 55% for power delivery larger than 2 W whereas the efficiency reaches between 67.5% and 77.5% for high-power delivery above 4 W. Higher power system can be implemented by increasing the supply voltage. Increasing the coupling will improve the efficiency of the system. This is achieved by either decreasing the transmitting coil size or increasing the receiving coil size. However, this may decrease the degree of freedom of movement on the planar surface and thus defeat the purpose of a loosely coupled magnetic induction power system.

This technology can be applied to rugged electronics to enable the creation of hermetically sealed units, eliminating the problem of charging port contamination and corrosion. In environments where sparking and arcing hazards exist, this technology can be applied since it eliminates external metallic contacts of electronic devices.

References

[1] L. Collins, "Cutting the cord," *Engineering and Technology*, vol. 2, no. 6, pp. 30–33, 2007.

[2] Z. N. Low, R. A. Chinga, R. Tseng, and J. Lin, "Design and analysis of a loosely coupled planar wireless power transfer system using magnetic induction," *IEEE Transactions on Industrial Electronics*, vol. 56, no. 5, pp. 1801–1812, 2009.

[3] R. Laouamer, M. Brunello, J. P. Ferrieux, O. Normand, and N. Bucheit, "A multi-resonant converter for non-contact charging with electromagnetic coupling," in *Proceedings of the 23rd International Conference on Electronics, Control and Instrumentation*, vol. 2, pp. 792–797, November 1997.

[4] H. Abe, H. Sakamoto, and K. Harada, "A non-contact charger using a resonant converter with parallel capacitor of the secondary coil," in *Proceedings of the Applied Power Electronics Conference and Exposition*, vol. 1, pp. 136–141, February 1998.

[5] G. Wang, W. Liu, M. Sivaprakasam, and G. A. Kendir, "Design and analysis of an adaptive transcutaneous power telemetry for biomedical implants," *IEEE Transactions on Circuits and Systems I*, vol. 52, no. 10, pp. 2109–2117, 2005.

[6] Y. Lu, K. W. E. Cheng, Y. L. Kwok, K. W. Kwok, K. W. Chan, and N. C. Cheung, "Gapped air-cored power converter for intelligent clothing power transfer," in *Proceedings of the 7th International Conference on Power Electronics and Drive Systems*, pp. 1578–1584, November 2007.

[7] Y. Jang and M. M. Jovanovic, "A contactless electrical energy transmission system for portable-telephone battery chargers," *IEEE Transactions on Industrial Electronics*, vol. 50, no. 3, pp. 520–527, 2003.

[8] C.-S. Wang, G. A. Covic, and O. H. Stielau, "Power transfer capability and bifurcation phenomena of loosely coupled inductive power transfer systems," *IEEE Transactions on Industrial Electronics*, vol. 51, no. 1, pp. 148–157, 2004.

[9] C.-S. Wang, G. A. Covic, and O. H. Stielau, "Investigating an LCL load resonant inverter for inductive power transfer applications," *IEEE Transactions on Power Electronics*, vol. 19, no. 4, pp. 995–1002, 2004.

[10] C.-S. Wang, O. H. Stielau, and G. A. Covic, "Design considerations for a contactless electric vehicle battery charger," *IEEE Transactions on Industrial Electronics*, vol. 52, no. 5, pp. 1308–1314, 2005.

[11] G. A. Kendir, W. Liu, G. Wang, et al., "An optimal design methodology for inductive power link with Class-E amplifier," *IEEE Transactions on Circuits and Systems I*, vol. 52, no. 5, pp. 857–866, 2005.

[12] U.-M. Jow and M. Ghovanloo, "Design and optimization of printed spiral coils for efficient transcutaneous inductive power transmission," *IEEE Transactions on Biomedical Circuits and Systems*, vol. 1, no. 3, pp. 193–202, 2007.

[13] J. T. Boys, G. A. Covic, and A. W. Green, "Stability and control of inductively coupled power transfer systems," *IEE Proceedings*, vol. 147, no. 1, pp. 37–42, 2000.

[14] G. A. Covic, G. Elliott, O. H. Stielau, R. M. Green, and J. T. Boys, "The design of a contact-less energy transfer system for a people mover system," in *Proceedings of the International Conference on Power System Technology*, pp. 79–84, December 2000.

[15] G. A. J. Elliott, J. T. Boys, and A. W. Green, "Magnetically coupled systems for power transfer to electric vehicles," in *Proceedings of the International Conference on Power Electronics and Drive Systems*, pp. 797–801, February 1995.

[16] X. Liu and S. Y. R. Hui, "Optimal design of a hybrid winding structure for planar contactless battery charging platform," *IEEE Transactions on Power Electronics*, vol. 23, no. 1, pp. 455–463, 2008.

[17] X. Liu and S. Y. R. Hui, "An analysis of a double-layer electromagnetic shield for a universal contactless battery charging platform," in *Proceedings of the 36th IEEE Power Electronics Specialists Conference*, pp. 1767–1772, June 2005.

[18] N. O. Sokal, "Class-E RF power amplifiers," *QEX*, pp. 9–20, 2001.

[19] F. H. Raab, "Effects of circuit variations on the class E tuned power amplifier," *IEEE Journal of Solid-State Circuits*, vol. 13, no. 2, pp. 239–247, 1978.

[20] F. H. Raab, "Idealized operation of the class E tuned power amplifier," *IEEE Transactions on Circuits and Systems*, vol. 24, no. 12, pp. 725–735, 1977.

[21] X. Liu, W. M. Ng, C. K. Lee, and S. Y. R. Hui, "Optimal operation of contactless transformers with resonance in secondary circuits," in *Proceedings of the 23rd Annual IEEE Applied Power Electronics Conference and Exposition*, pp. 645–650, February 2008.

[22] J. J. Casanova, Z. N. Low, J. Lin, and R. Tseng, "Transmitting coil achieving uniform magnetic field distribution for planar wireless power transfer system," in *Proceedings of the IEEE Radio and Wireless Symposium*, pp. 530–533, January 2009.

[23] M. Ahn, C.-H. Lee, and J. Laskar, "CMOS high power SPDT switch using multigate structure," in *Proceedings of the IEEE International Symposium on Circuits and Systems*, pp. 3283–3286, May 2007.

[24] M. Yu, R. J. Ward, and G. M. Hegazi, "High power RF switch MMICs development in GaN-on-Si HFET technology," in *Proceedings of the IEEE Radio and Wireless Symposium (RWS '08)*, pp. 855–858, January 2008.